Journal of ELECTRONIC MATERIALS, Vol. 45, No. 11, 2016
DOI: 10.1007/s11664-016-4765-1

A High Efficiency Boost Converter with MPPT Scheme for Low Voltage Thermoelectric Energy Harvesting

MINGJIE GUAN,[1] KUNPENG WANG,[1] QINGYUAN ZHU,[1] and WEI-HSIN LIAO[2,3]

1.—School of Aerospace Engineering, Xiamen University, Xiamen, Fujian, China. 2.—Department of Mechanical and Automation Engineering, The Chinese University of Hong Kong, Shatin, N.T, Hong Kong, China. 3.—e-mail: whliao@cuhk.edu.hk

Using thermoelectric elements to harvest energy from heat has been of great interest during the last decade. This paper presents a direct current–direct current (DC-DC) boost converter with a maximum power point tracking (MPPT) scheme for low input voltage thermoelectric energy harvesting applications. Zero current switch technique is applied in the proposed MPPT scheme. Theoretical analysis on the converter circuits is explored to derive the equations for parameters needed in the design of the boost converter. Simulations and experiments are carried out to verify the theoretical analysis and equations. A prototype of the designed converter is built using discrete components and a low-power microcontroller. The results show that the designed converter can achieve a high efficiency at low input voltage. The experimental efficiency of the designed converter is compared with a commercial converter solution. It is shown that the designed converter has a higher efficiency than the commercial solution in the considered voltage range.

Key words: Thermoelectric, boost converter, maximum power point tracking, efficiency

INTRODUCTION

Wireless sensors have being widely used in monitoring the human body, buildings, transportation, and remote areas. These sensors are usually powered by traditional batteries. One drawback of the battery-powered system is to recharge or replace the battery when the energy stored in the battery has run out. In many applications, replacing batteries is inconvenient and cost ineffective. In recent years, energy harvesting technologies from the environment have been growing rapidly. The environmental energy sources for energy harvesting can be vibration, thermal, solar, and radio frequency (RF) energy. While there are several options for obtaining the ambient energy, thermoelectric transducers have attracted more attention, especially in the applications of wearable sensors[1] and smart buildings.[2]

(Received March 18, 2016; accepted June 18, 2016; published online July 11, 2016)

However, the major limitation encountered in thermoelectric energy harvesting for wireless sensors is that the output voltage of the thermoelectric generator (TEG) element is usually too small for direct use. Therefore, boost converters are needed to boost the voltage to a higher level for wireless sensor use. In order to fulfill high efficiency for the boost converter, impedance matching is usually applied to the converter. Through impedance matching, the input impedance of the converter will be equal to the internal resistance of the TEG element, and the input voltage of the converter circuit will be one half of the open-circuit voltage of the TEG element. Maximum power point tracking (MPPT) schemes are usually used in direct current–direct current (DC–DC) converters for impedance matching. A lot of research has been done on the MPPT schemes for the thermoelectric energy harvester. Park et al.[3] proposed a MPPT scheme using an analog circuit without a microcontroller unit. However, their scheme was shown only with

simulation results. No experimental results were shown for verification. Gao et al.[4] and Wu et al.[5] applied DC–DC converters with a MPPT scheme in their TEG systems with the use of the perturbation and observation algorithm. However, their converter and controller were designed towards high input current and high input voltage applications, which is not acceptable for a low power and low voltage harvesting system. Maganga et al.[6] implemented two MPPT algorithms (perturbation and observation algorithm and extremum seeking control algorithm) to control a DC–DC converter for thermoelectric generators. A portable digital signal processing and control engineering (dSPACE) device was used in realizing the algorithms. However, the power consumption of the control system was not shown in the paper. Chen and Fan[7] presented a 100 mV input, 500 mV output, single-inductor multiple-output based DC–DC converter for thermoelectric energy harvesting. However, the output voltage of 500 mV is too low for a wireless sensor. Carlson et al.[8] proposed a converter circuit that can convert a small input voltage of 20 mV to a regulated 1-V output. Kim and Kim[9] presented a DC–DC boost converter with MPPT technique for thermoelectric energy harvesting applications. The technique realized variation tolerance by adjusting the switching frequency of the converter. However, both of the power consumptions of the controllers in Refs. 8 and 9 were not shown in their papers.

There are also some commercial boost converters, which were designed for low-power energy harvesting systems. LTC3108 from Linear Technology[10] can operate at very low input voltage (as low as 20 mV), by employing resonant converter topology with an external transformer. However, it does not possess a MPPT scheme. Therefore, its efficiency is relatively low at no more than 40%. BQ25504 from Texas Instruments[11] needs a relatively higher input voltage of 80 mV, using boost converter topology with a MPPT scheme. As a result, it has a higher efficiency in its operating input voltage range. In this paper, a high efficiency switching DC–DC boost converter with the MPPT control technique for low input voltage is proposed. Unlike other MPPT techniques to adjust the switching frequency, our MPPT technique precisely adjusts the on–off time of the switches in the boost converter according to the open-circuit voltage to fulfill a zero current switch (ZCS) technique and high efficiency for the converter.

This paper is organized as follows. In the "System Design and Theoretical Analysis" section, the design of the thermal energy harvesting system and theoretical analysis of the converter and parameters are described. Equations for the parameters needed in the ZCS technique are derived. In "Simulations" section, simulations of the converter using PSPICE software are performed to verify the theoretical equations. The experiments and measurement results are given in "Experiments and Results" section for comparison with theoretical analysis and simulation results. Finally, conclusions and discussions are presented in "Conclusions and Discussions" section.

SYSTEM DESIGN AND THEORETICAL ANALYSIS

A simplified thermoelectric energy harvesting system with a DC–DC converter is shown in Fig. 1. The thermoelectric element can be modeled as a voltage source V_T in series with its internal resistance R_T. The amplitude of the voltage V_T varies with the temperature difference level between the hot and cold junctions of the thermoelectric element. The internal resistance R_T is slightly changed depending on the temperature difference level.[4] The optimal power output of the TEG occurs when the input resistance R_{in} matches the internal resistance R_T.

The optimal value of the input voltage V_{i_opt} is one half the open-circuit voltage of the thermoelectric generator V_T. When the open circuit voltage is measured, the voltage V_{i_opt} can be determined. The optimal input power to the converter at input voltage V_{i_opt} is

$$P_{i\_opt} = V_{i\_opt} I_{i\_opt} = V_{i\_opt} \cdot \left(\frac{V_T - V_{i\_opt}}{R_T} \right) = \frac{V_{i\_opt}^2}{R_T}. \quad (1)$$

To harvest the power from a varying voltage source of TEG, the architecture of our harvesting system is shown in Fig. 2. The power from the thermoelectric element was firstly charged to an input capacitor C_i whose voltage was kept at the optimal input voltage V_{i_opt} and then transferred to an output capacitor C_o through our designed boost DC–DC converter. To implement the MPPT scheme, the harvesting circuit was periodically disconnected from the TEG element by the switch G_0, and the open-circuit voltage was measured during the short disconnection period by a voltage measurement unit. A controller was applied to finely control the switches in the converter.

The DC–DC converter applied in the harvesting system is shown in Fig. 3. The converter consisted of an inductor L and two controlled on–off switches G_1 and G_2. A freewheel diode in a conventional boost

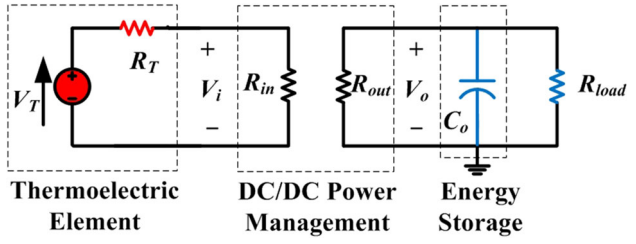

Fig. 1. Simplified thermoelectric energy harvesting system.

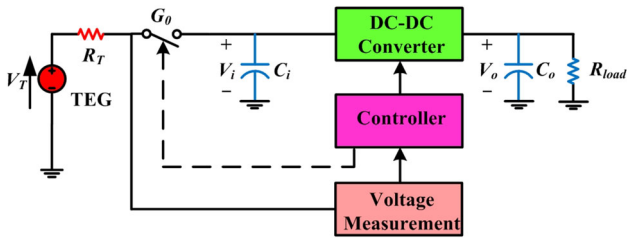

Fig. 2. Thermoelectric energy harvesting system with MPPT technique.

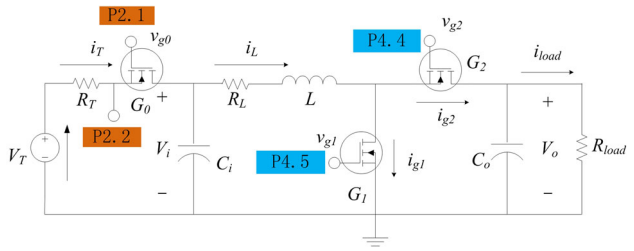

Fig. 3. DC–DC converter topology in our energy harvesting system.

converter was replaced by the switch G_2 to lower the power loss from the voltage drop of the freewheel diode. In general, the switches G_1 and G_2 can be metal-oxide semiconductor field-effect transistors (MOSFETs). In order to accomplish high efficiency, the ZCS technique was implemented by turning on/off the switches when the switch currents were near zero to lower the reverse current loss and body conduction loss of the power switches. Unlike other ZCS techniques using a current sensing circuit, in our technique the on/off time of the switches is theoretically calculated and controlled by the controller based on the derived theoretical equations. Without an external current sensing circuit and its power loss, higher converter efficiency could be achieved in our converter.

The operating procedures and waveforms of the converter in the ZCS technique are shown in Figs. 4 and 5, respectively. The capacitor C_i was charged from the beginning. When the voltage of the capacitor C_i reached the optimal value, the converter started to transfer the energy on the capacitor C_i to the capacitor C_o. The switches in the converter were controlled to switch on or off to keep the voltage of the capacitor C_i optimal. When switch G_1 was switched on and switch G_2 was switched off (see Fig. 4a), the current i_L gradually increased from zero because of the presence of the inductor L. When the voltage v_{g1} fell to zero and v_{g2} rose to a high level, the switch G_1 was switched off and switch G_2 was switched on again (see Fig. 4b). The current i_L decreased to zero in the interval t_2.

As shown in Fig. 5, during the internal t_1, the current linearly increased with time; there will be

$$\frac{\Delta i_L}{t_1} = \frac{V_i - i_L R_L - V_{on1}}{L} = \frac{i_{Lm}}{t_1}, \qquad (2)$$

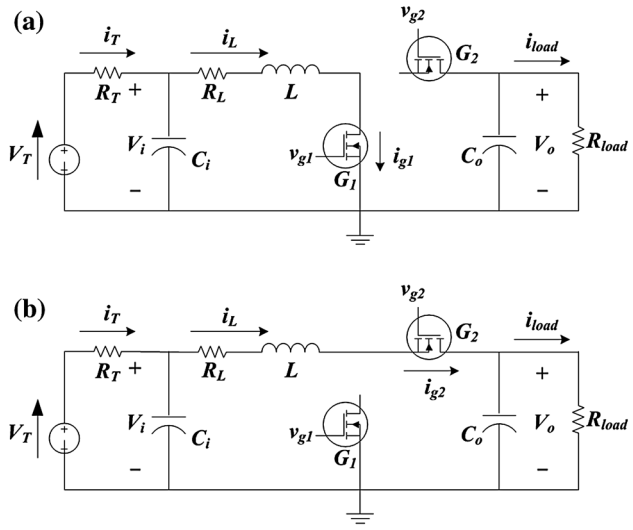

Fig. 4. Converter operations (a) switch G_1 is "on" and switch G_2 is "off" (b) switch G_1 is "off" and switch G_2 is "on".

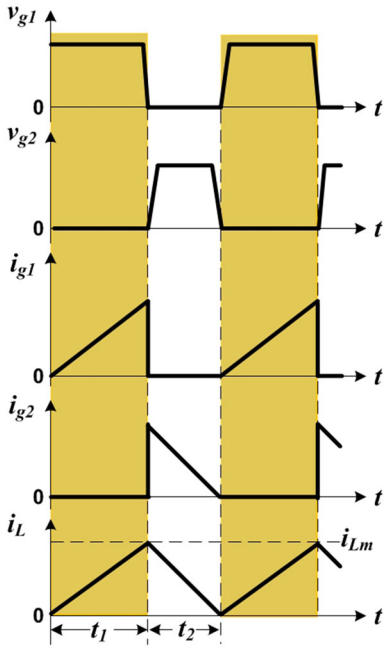

Fig. 5. Waveforms of the voltages and currents in the converter.

where L is the inductance; i_{Lm} is the peak current of the inductor; and V_{on1} is the switch-on voltage of the switch G_1.

To keep the voltage of the capacitor C_i optimal, the average current $\overline{i_L}$ should be equal to the current I_{i_opt} in Eq. 1. In the theoretical analysis, the voltage drop from the internal resistance of the inductor $i_L R_L$ is not considered. This will be

$$\frac{V_i - V_{on1}}{L} = \frac{i_{Lm}}{t_1} = \frac{2\overline{i_L}}{t_1} = \frac{2V_i}{R_T t_1}. \qquad (3)$$

From Eqs. 2 and 3, this will be

$$t_1 = \frac{2L}{R_T} \times \frac{V_i}{V_i - V_{on1}}. \quad (4)$$

In the interval t_2, the current i_L will linearly decrease from i_{Lm} to zero with time. This will be

$$\frac{\Delta i_L}{t_2} = -\frac{V_i - i_L R_L - (V_{on2} + V_o)}{L} = \frac{i_{Lm}}{t_2}. \quad (5)$$

By ignoring the voltage drop due to the internal resistance of the inductor $i_L R_L$, this will be

$$\frac{V_o - V_i + V_{on2}}{L} = \frac{i_{Lm}}{t_2} = \frac{2V_i}{R_T t_2}. \quad (6)$$

From Eqs. 5 and 6, this will be

$$t_2 = \frac{2L}{R_T} \times \frac{V_i}{V_o - V_i + V_{on2}}. \quad (7)$$

The average current flowing through the load R_{load} is

$$\overline{i_{load}} = \frac{V_i - V_{on1}}{2(V_o - V_{on1} + V_{on2})} i_{Lm}. \quad (8)$$

Thus, the theoretical efficiency of the converter can be expressed as

$$\eta_c = \frac{\overline{i_{load}} \times V_o}{\overline{i_L} \times V_i} = \frac{V_i - V_{on1}}{V_o + V_{on2} - V_{on1}} \times \frac{V_o}{V_i}. \quad (9)$$

From Eq. 9, it can be found that the efficiency is related to the parameters of V_i, V_o, V_{on1} and V_{on2}. The switching period T_s is

$$T_s = t_1 + t_2 = \frac{2L}{R_T} \times \left(\frac{V_i}{V_i - V_{on1}} + \frac{V_i}{V_o - V_i + V_{on2}} \right). \quad (10)$$

The duty cycle of the control voltage of the gate G_1 is

$$DC_1 = \frac{t_1}{t_1 + t_2} = \frac{V_o + V_{on2} - V_i}{V_o - V_{on1} + V_{on2}}. \quad (11)$$

The duty cycle of the control voltage of the gate G_2 is

$$DC_2 = \frac{t_2}{t_1 + t_2} = \frac{V_i - V_{on1}}{V_o - V_{on1} + V_{on2}}. \quad (12)$$

The output voltage V_o is related to the resistance of the load resistor. A load resister with smaller resistance will decrease the output voltage. The load resistance R_{load} can be determined by

$$R_{load} = \frac{V_o^2}{\eta_c V_i^2} R_T. \quad (13)$$

SIMULATIONS

Simulations were carried out to verify the derived theoretical equations. The boost converter circuit built in PSPICE software is shown in Fig. 6. A voltage source V_{teg} with internal resistance R_T was used as a simulated TEG in the simulation. The internal resistance could be from several ohms to hundreds of ohms. R_T was set as 47 Ω as an example. Other parameters in the simulation are given as follows: the inductance L was set as 1 mH; the internal resistance of the inductor R_L was set as 1.12 Ω; the input capacitor C_i was set as 10 μF; the output capacitor C_o was set as 1 μF; G_1 and G_2 were both n-channel metal–oxide–semiconductor field-effect transistors (NMOSs), modeled *BSS138*/FAI; and v_{g1} and v_{g2} were the control voltages.

The first simulation was to validate the optimal t_1 and t_2 expressed in Eqs. 4 and 7. Using the V_T of 0.3 V, the optimal input voltage V_i should be 0.15 V. The high level, low level, rise time, and fall time of control voltages v_{g1} and v_{g2} were set as 3 V, 0 V, 0.1 μs, and 0.1 μs, respectively. The control voltages v_{g1} and v_{g2} were applied to the switches when V_i reached 0.15 V. After that moment, the switch "SW" was switched on. Switch-on voltages V_{on1} and V_{on2} of the NMOSs G1 and G2 were set as 0.01 V and 0.03 V, respectively, which were based on the real performance of the chosen components.

The output voltage was targeted as one and a half volts in the first simulation. The optimal t_1 and t_2 were theoretically determined to be 45.6 μs and 4.6 μs by Eqs. 4 and 7. The period of the control voltage v_{g1} and v_{g2} were both 50.6 μs. The theoretical control frequency f_s, duty cycles DC_1 and DC_2 were 19.763 kHz, 90.12% and 9.09%, respectively. From Eq. 13, R_{load} was determined to be 5.875 kΩ.

The resulting input voltage and output voltage of the DC–DC converter from 0 s to 14 ms are shown in Fig. 7 using the above parameters. In Fig. 7, the input voltage of the simulation is shown as the blue dash-dot line and the output voltage of the simulation is shown as the black dash line. From the simulation results, it can be seen that the input voltage is kept at the target optimal voltage of 0.15 V, and the output voltage can reach the target output voltage 1.5 V in a short time.

Another simulation was performed to validate the efficiency equation for different V_T. The amplitude of the V_T was set from 0.15 V to 1 V. For each V_T, the input voltage was kept optimal from 75 mV to 500 mV by modulating t_1 and t_2 based on Eqs. 4 and 7. The target output voltage was all set to be 1.5 V. From Eq. 13, the resistor R_{load} was specified for each V_T. With Eq. 9, the theoretical efficiency of the converter is drawn as shown in the blue solid curve in Fig. 8. The efficiency can also be calculated from

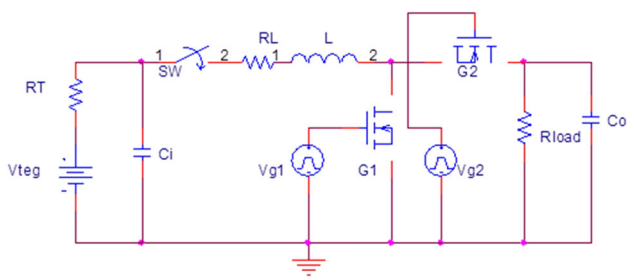

Fig. 6. Boost converter circuit built in PSPICE simulation.

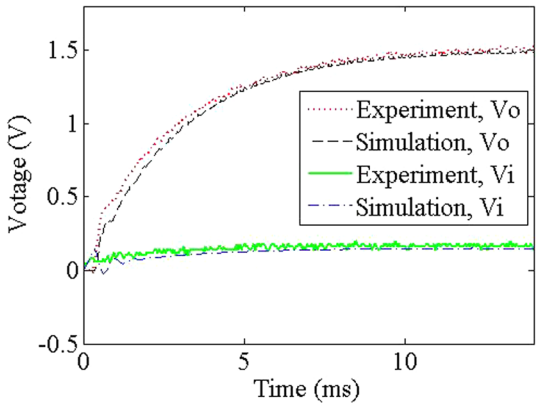

Fig. 7. Simulation and experimental results of input and output voltages.

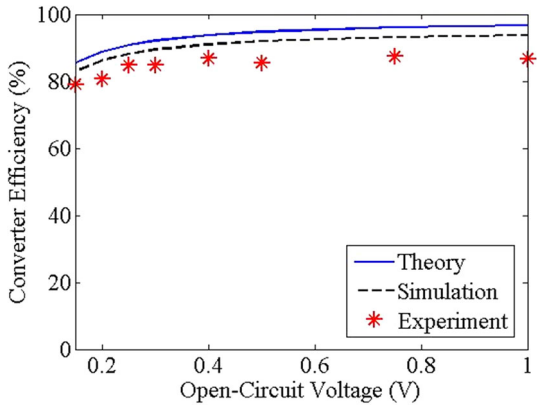

Fig. 8. Efficiencies of the designed converter.

the simulation results. In simulation, the input power is obtained from the input voltage and the input current; the output power is obtained from the power consumption of the R_{load}; the converter efficiency is determined from the ratio of the output power to input power. The simulation results are shown in Fig. 8 as the black dash line.

It can be seen from Fig. 8 that the theory curve and the simulation curve match well with the simulation curve some below the theory curve. The reason for the drop in simulation efficiency may be from that in the theoretical calculation the resistive loss of the inductor resistance R_{L} is neglected, but in the simulation it is considered.

EXPERIMENTS AND RESULTS

Experiments were carried out to verify the theoretical equations and simulation results of the proposed system. The proposed converter circuit was implemented with discrete components, as shown in Fig. 9. The inductor is model SLF12555T-102 from TDK Co. The NMOSs are model BSS138 from Fairchild Semiconductor Co. A low-power MSP430 controller model MSP430F2274 was used as the controller. The input/output (I/O) ports of the controller in connection with our developed converter circuit are shown in Fig. 3. Control voltages V_{g0}, V_{g1} and V_{g2} were connected to I/O port P2.1, P4.5, P4.4 of the controller, respectively. The V_{T} of the TEG was sampled by I/O port P2.2 of the controller. For convenience, a voltage source and an adjustable resistor were used to emulate the thermoelectric element in the experiments. In order to compare our designed converter with a commercial solution, i.e., BQ25504 from Texas Instruments by experiments, a DC–DC converter based on a purchased BQ25504 chip was also built on the same circuit board as shown in Fig. 9. The BQ25504 converter was built based on the typical TEG application circuit described in the datasheet of the BQ25504 chip.[11] The built BQ25504 converter also possessed the MPPT ability

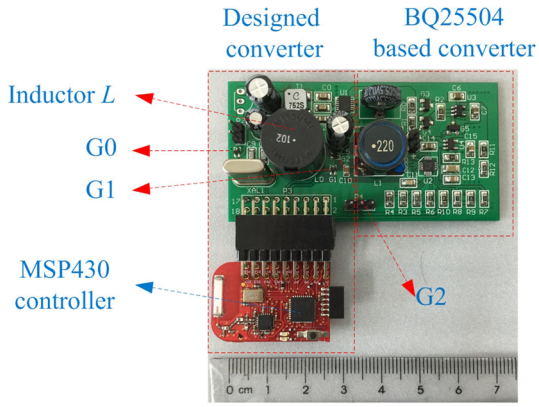

Fig. 9. Built converter circuits in experiments.

by setting the input voltage as half of the open-circuit voltage.

During the experiment, the open-circuit voltages were sampled and transferred to the 10-bit analog-to-digital converter with sample-and-hold embedded in the MSP430 controller. The control voltages V_{g0}, V_{g1} and V_{g2} were generated by the controller based on the theoretical equations of t_1, t_2 and T_{s}. The input/output voltages and the control voltages were recorded by a data acquisition unit. For example, during the boost stage (output voltage lower than the target voltage), the output voltage and the control voltage V_{g2} are shown in Fig. 10. It can be seen from Fig. 10 that when the voltage V_{g2} is at a high level, the output voltage has a small increase towards the target voltage.

Experiments on the time responses of the input/output voltages were explored first. The V_{T} of the voltage source was set as 300 mV. A resistor of 47 Ω was connected in series with the voltage source to emulate the TEG element. The value of the internal resistance was the same as that used in the simulation. The measurement results of input/output voltages are demonstrated as green solid line and red dot line as shown in Fig. 7 for comparison with the simulation results. From Fig. 7, it is

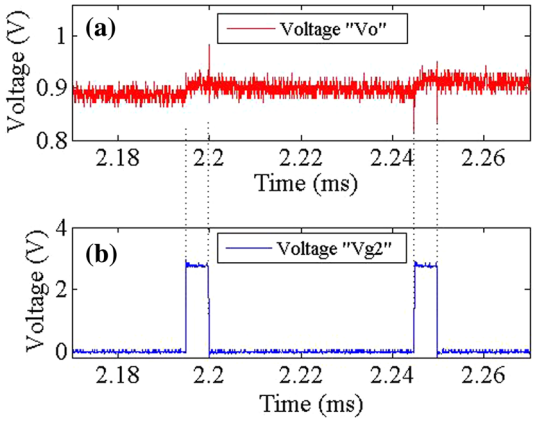

Fig. 10. Output voltage "V_o" and control voltage "V_{g2}" during the boost stage (a) output voltage "V_o" versus time (b) control voltage "V_{g2}" versus time.

observed that the experimental curve fits well the simulation curve.

Experiments on the conversion efficiency of the converter for a range of input voltages were explored. The V_T of the voltage source was set from 150 mV to 1 V. A resistor of 47 Ω was used as the internal resistance for comparison with the simulation results. The measurement results of conversion efficiency under different open-circuit voltages are demonstrated as the star-marked points in Fig. 8. From Fig. 8, it is observed that the experimental data are comparable with the theoretical calculation and the simulation curve. However the experimental efficiencies are lower than the simulation results because some power losses exist in experiments but are not considered in the simulation. The performances of the real components such as NMOS switches and inductor would be more complicated than their simplified models in the PSPICE software would perform. Nonetheless, our converter achieves high efficiencies in the experiments. The lowest and highest efficiencies of converter are 80.3% and 86.3% in the considered voltage range.

To compare our designed converter with the commercial converter BQ25504, two resistors, 10 Ω and 47 Ω, were used to emulate normal internal resistance and high internal resistance of the TEG, respectively. The V_T was set from 150 mV to 1 V. For our designed converter, the output voltage was set as 1.5 V. For BQ25504, the output voltage was also set as 1.5 V. The experimental efficiency results are compared and shown in Fig. 11.

From Fig. 11, it is observed that our converter efficiencies are higher than the converter efficiencies of BQ25504 for both low and high internal resistance, especially in the low voltage range (150 ~ 400 mV). It is also observed that the efficiency of our designed converter is not sensitive to the internal resistance, whereas the efficiency of the BQ25504 converter has a larger difference towards the internal resistance for each V_T. It means the

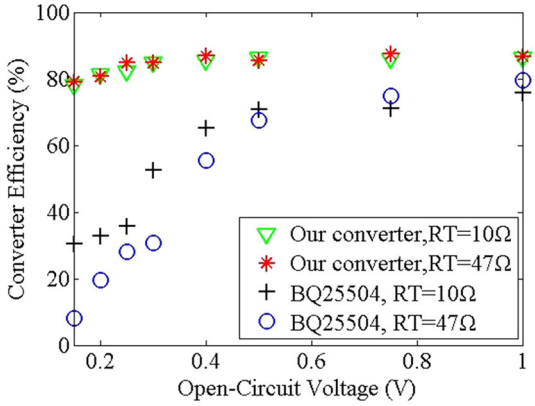

Fig. 11. Efficiency comparison of our converter with BQ25504.

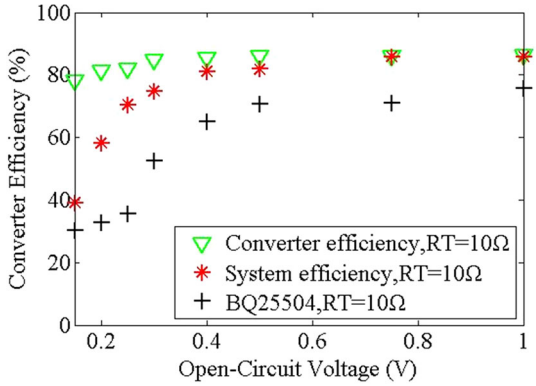

Fig. 12. Comparison of converter efficiency, system efficiency with BQ25504.

MPPT ability of our designed converter is better than BQ25504.

However, the controller of the BQ25504 is self-contained, whereas our converter needs an external microcontroller. In the experiments, the power consumption of our controller was in the range of 200 ~ 225 μW. Our converter efficiency and overall system efficiency by wiping out the power consumption of the controller are compared with the BQ25504 converter towards a 10 Ω internal resistance in Fig. 12. From Fig. 12, it is shown that our overall system efficiency is still higher than the BQ25504 converter in the considered voltage range. Moreover, if the power consumption of our microcontroller could be lowered, the overall system efficiency would be even higher. Lowering the power consumption of our controller is still on-going. Our target is to lower the power consumption of our controller to be smaller than 100 μW.

CONCLUSIONS AND DISCUSSIONS

A DC–DC boost converter with a MPPT scheme for thermoelectric generators with high efficiency at low input voltage was presented in this paper. The MPPT scheme controls the on/off

time intervals of the switches according to the open-circuit voltage of the thermoelectric generator. The on–off switches were controlled to fulfill a ZCS technique to decrease power loss and achieve high efficiency.

Expressions of the optimal on/off time intervals of controlled switches, switching frequency, duty cycles, optimal load resistance and efficiency of the converter were derived. Simulations and experiments were explored to verify the ZCS technique in the MPPT scheme and the theoretical equations. From the experimental results, it was shown that a high efficiency of 80.3% $\sim$ 86.3% can be achieved by our boost converter with an open-circuit voltage of 0.15 V $\sim$ 1 V to an output voltage of 1.5 V. The higher efficiency comes from the combined effects of both the ZCS technique and the better matched passive components including the inductor and the NMOS switches. In this paper, the effect of the ZCS technique was shown. However, the effect from the better matched passive components is still under investigation.

The controller of the energy harvesting system will consume a part of the harvested energy. Considering the power consumption of the controller, our overall system efficiency is still higher than the commercial BQ25504 converter, especially in the low voltage range below 400 mV. Provided that the consumed power in the controller could be reduced in the future, the overall system efficiency could be even higher.

ACKNOWLEDGEMENTS

The work described in this paper was supported by a Grant from the China Science Foundation (Project No. 51575463) and a grant from the Innovation and Technology Commission of Hong Kong Special Administrative Region, China (Project No. ITS/248/14FP).

REFERENCES

1. V. Leonov, *IEEE Sens. J.* 13, 2284 (2013).
2. J.W. Matiko, N.J. Grabham, S.P. Beeby, and M.J. Tudor, *Meas. Sci. Technol.* 25, 012002 (2014).
3. J. Park and S. Kim, *J. Electron. Mater.* 41, 1242 (2012).
4. J. Gao, K. Sun, L. Ni, M. Chen, Z. Kang, L. Zhang, Y. Xing, and J. Zhang, *J. Electron. Mater.* 41, 1043 (2012).
5. H. Wu, K. Sun, J. Zhang, and Y. Xing, *J. Electron. Mater.* 42, 1737 (2013).
6. O. Maganga, N. Phillip, K.J. Burnham, A. Montecucco, J. Siviter, A. Knox, and K. Simpson, *J. Electron. Mater.* 42, 1900 (2013).
7. P.H. Chen and M.Y. Fan, *IEEE Trans. Circuit. Syst.-I* 62, 405 (2014).
8. E.J. Carlson, K. Strunz, and B.P. Otis, *IEEE J. Solid State Circ.* 45, 741 (2010).
9. J. Kim and C. Kim, *IEEE Trans. Power Electron.* 28, 3827 (2013).
10. Linear Technology, LTC 3108 datasheet, 2010. http://cds.linear.com/docs/en/datasheet/3108fc.pdf.
11. Texas Instruments, BQ25504 datasheet, 2012. http://www.ti.com/lit/ds/symlink/bq25504.pdf.